Journal of Sound and Vibration 333 (2014) 2390–2403

Contents lists available at ScienceDirect

Journal of Sound and Vibration

journal homepage: www.elsevier.com/locate/jsvi

# Fundamental frequency evolution in slender beams subjected to imposed axial displacements

A. Carpinteri [a], R. Malvano [b], A. Manuello [a], G. Piana [a,*]

[a] Department of Structural, Geotechnical and Building Engineering, Politecnico di Torino, Corso Duca degli Abruzzi 24, I-10129 Torino, Italy
[b] INRIM – Fluid Dynamics Unit C/o DIMEAS, Politecnico di Torino, Corso Duca degli Abruzzi, 24, I-10129 Torino, Italy

ARTICLE INFO

*Article history:*
Received 17 January 2013
Received in revised form
20 January 2014
Accepted 22 January 2014
Handling Editor: S. Ilanko
Available online 18 February 2014

ABSTRACT

The influence of applied axial loads on the fundamental vibration frequency is strictly connected with the stability analysis of elastic slender beams. For this reason, the correct evaluation of the fundamental frequency is of primary importance in designing new structures and components, as well as in monitoring existing ones. At the same time, if an internal axial load arises in a slender element as the consequence of an imposed (static) axial end displacement, then a different dynamic structural response is encountered respect to the case in which a beam end is free to slide, during transverse vibration, and a (constant) axial load is applied externally. This difference is due to the change in the axial boundary condition. Moreover, the presence of an initial curvature of the beam axis may significantly affect the aforesaid response. The experimental study proposed in the present paper investigates the dependence of the fundamental frequency on the axial load in slender beams subjected to imposed axial end displacements. The considered specimens presented different geometrical imperfections (initial curvatures), and were tested in two different constraint conditions (hinged–hinged and hinged–clamped). In addition, the behaviors observed during the experiments were reproduced by numerical simulations offering a valid confirmation for test results and contributing to understand the evolution of the fundamental frequency in the analyzed slender elements subjected to imposed axial end displacements.



## 1. Introduction

A very large number of engineering problems in structural dynamics, both in linear and nonlinear ranges, have been studied during the last decades, and powerful methods have been developed for different structural elements subjected to different loading conditions [1–3]. In addition, the influence of the applied loads on the natural frequencies is one of the most investigated problems [4]. Early studies were focused on transverse vibrations of elastic beams under constant axial loads [5–12], these were then followed by more and more refined analyses, regarding beams, arches, plates and shells [13–33]. As is well known, the problem of the influence of applied loads on the natural vibration frequencies is strictly connected with the analysis of the stability of the elastic equilibrium of mechanical systems and structures. In particular, the

* Corresponding author.
*E-mail addresses:* gianfranco.piana@polito.it, gianfrancopiana@tiscali.it (G. Piana).

http://dx.doi.org/10.1016/j.jsv.2014.01.018
0022-460X 

zero-frequency condition corresponds to the loss of stability by divergence (static instability), and it furnishes the critical buckling load (or load group multiplier) [34–38]. On this basis, the experimental determination of instability loads of columns and structures by non-destructive vibration tests have been performed, by different authors, for different structural configurations, such as column-type and thin-walled structures [4,39–41]. The unifying approach of these studies is to consider the influence of applied loads on natural vibration frequencies of slender structures. On the other hand, a different influence of the axial load on the natural frequencies is obtained, respect to the previous case, when the axial load is induced in a slender element by an imposed axial displacement, rather than directly applied from outside, because of the difference in the axial boundary condition. These effects – less infrequent than we might think – may appear when slender structures are subjected to external moving constraints. For example, for bridges and large structures the reduction in bearing capacity and the sudden collapse of compressed elements can be the result of constraint settlements or structural subsidence due to seismic events. Also, a situation analogous to that of a prescribed axial displacement in a slender beam is obtained when, for example, a uniform thermal expansion is restrained.

In case of prescribed axial displacement, the internal axial load varies (oscillates) during the beam vibration, due to the change in axial strain; consequently, the variation of the frequency with the axial load will differ from that of the case in which a beam end is free to slide and a (constant) axial load is applied from outside [42,43]. Furthermore, when both ends are axially restrained, the presence of an initial curvature contributes to the stiffness of the beam which behaves like a pinned shallow arch [44–48]. Dickinson [44] studied the effect of the induced axial loads upon the natural frequencies of flexural vibration in initially slightly curved beams subjected to prescribed axial end displacement. In that paper, two end conditions were examined (pinned–pinned and clamped–clamped), and it was shown that the effect of relatively slight initial lack of straightness upon the induced axial load and bending frequencies is very significant. In determining the axial load induced by the prescribed axial end displacement, the initial deflection was assumed having the form of the fundamental critical buckling mode, while the frequencies were determined adopting straight beam theory in the vibration analysis. The latter assumption resulted in restricting the applicability of the analysis to very small initial curvatures and vary small axial end displacements. The problem was re-examined by Kim and Dickinson [45], this time including the effect of initial curvature in the vibration analysis.

Yamaki and Mori [46] studied the nonlinear vibrations of a clamped beam with initial deflection and initial axial displacement under a uniformly distributed periodic load. In that paper, the authors also solved their more general equations to obtain the linear natural frequencies of the beam taking into consideration the effects of initial deflection and initial axial displacement.

Ilanko [47] investigated the effects of partial axial end restraints on the natural frequencies of initially slightly curved, simply supported beams subject to axial compressive force. In that paper, it was shown that the effect of the initial curvature on the natural frequencies depend on the axial end conditions. In particular, the presence of an initial curvature may induce a stiffening in the beam, causing it to behave like an arch, with a consequent increase in the natural frequencies respect to those of the corresponding straight beam. In that study, the initial lack of straightness was taken as a Fourier sine series. The work by Ilanko [47] may be related to the problem investigated in the present paper in the case when both beam ends are fully axially restrained.

Lastly, Hallauer and Ma [48] draw attention to the practical relevance of evaluating the influence of initial curvature and initial axial displacement upon the flexural vibration of slender beams in designing microbridge resonators adopted in sensing and acting devices.

In the present paper, we deal with an experimental investigation on the fundamental frequency evolution in slender steel beams subjected to axial displacements. Different geometrical imperfections, in terms of initial curvature, were considered in order to understand their influence on the evolution of the first natural frequency. In addition, each specimen was tested in two different constraint conditions. The tests were conducted using a servo-controlled testing machine under displacement-controlled condition. The experimental apparatus was realized according to metrological requirements and was fine tuned at the National Institute of Metrological Research (INRIM), while the experiments were carried out at the Experimental Laboratory of Materials and Structures of the Politecnico di Torino (MASTRLAB). For each specimen, the fundamental frequencies corresponding to different imposed displacements – and, therefore, to different axial loads – were evaluated analyzing both the free and forced responses: an electromagnet and a laser displacement transducer with suitable characteristics were adopted. Hence, the fundamental frequency versus axial load curves were obtained, therefore revealing a transition from a beam-like behavior to an arch-like behavior, with an increase in the beam stiffness as the load increases [45,47]. This transition may be used to discriminate between two different phases and to evaluate the stability of structural elements subjected to external conditions such as constraint subsidence: the achievement of particular values of the natural frequency may be used as a monitoring indicator in existing structures. In addition, numerical simulations were performed offering a valid interpretation of the experimental results and contributing to understand the phenomenon under investigation.

The present work distinguishes from the cited references on the subject [44–48], in addition to the peculiarities of the experimental setup and test procedure, mainly for the profile of the initial geometrical imperfection. Also, the pinned–clamped constraint condition has not been analyzed in the abovementioned references. Moreover, in this paper we show how the phenomenon under investigation can be numerically simulated in a multi-body framework, which can be conveniently applied as a valid alternative to the finite element method when an analytical solution is not available.

## 2. Experimental setup

### 2.1. Specimen preparation

The specimens used during the experimental tests consisted of three steel bars. All these elements present a rectangular cross-section 15 mm deep and 30 mm thick, and a length ($l$) equal to 1000 mm (Fig. 1). In order to evaluate the evolution of the fundamental vibration frequency with the axial load, considering different initial imperfections, these specimens were subjected to a preliminary phase where different geometrical configurations were realized. The first specimen, B1, is a rectified beam, with a maximum offset ($e_0$) from the ideal rectilinear condition no larger than 0.2 mm (i.e. a ratio $e_0/l \leq 0.2/1000$) (Fig. 1a). This configuration is assumed as the rectilinear one and will be used to compare the results obtained from the other specimens presenting larger geometrical deviations. For the other two specimens, different geometrical deviations were introduced imposing a prescribed offset from the rectilinear configuration. The profile of the initial deflection from straightness is linear in the end portions for a length equal to 15 cm, while it is parabolic in the central part. In particular, specimens B2 and B3 present a maximum offset at mid-length equal to 1 mm ($e_0/l=1/1000$) and 2 mm ($e_0/l=2/1000$), respectively (Fig. 1a). At both the ends of each specimen a spherical cavity was created, with a radius of 8 mm and a maximum depth of 2.5 mm, and centered with a tolerance of $\pm 0.1$ mm (Fig. 1b). These cavities are the place where two end spheres were positioned during the tests in order to facilitate the specimen centering and to realize the external constraints at the same time, as will be described better later on.

### 2.2. Specimen centering, experimental equipment and testing procedure

Fig. 2 shows a general view of the experimental setup. The experimental tests were conducted using a servo-controlled machine (MTS) with a closed-loop electronic control, having a maximum capacity of 100 kN. The specimen is positioned vertically and connected to the testing machine by two end joints that realize the external constraints. Two horizontal transverses are positioned at mid-height of the tested beam: one supports a laser displacement transducer (measuring device) and the other supports an electromagnet (forcing device). Both the electromagnet and the measuring device act without any contact with the specimen. The complete experimental apparatus is constituted by a wave generator, a signal amplifier, an oscilloscope, and a data acquisition device (Fig. 2).

Fig. 3 shows schemes and pictures of the two end joints that realize the external constraints of the tested beam. These joints are rigidly connected through a double-threaded pin to the testing machine, with steel rings that guarantee a correct transmission of the load (see Fig. 2b, c). While the upper joint remains in a fixed position, the lower one may be adjusted in the horizontal plane to allow the correct positioning therefore ensuring the vertical alignment. To ensure the required verticality, a steel element was created ad hoc for the verification of the alignment of the two joints and the correct assembly of the apparatus (Fig. 4). It consists of a straight bar of full-round circular cross-section, welded to a circular disk which, by construction, was made orthogonal to its longitudinal axis. The assessment was done using a level positioned along different orientations, and a self-leveling laser as shown in Fig. 4. The alignment is important to transmit displacements (and therefore, forces) along a direction as vertical as possible at the same time allowing the positioning of the specimen with its longitudinal axis in the vertical position. The adjustment of the position of the movable part of the lower joint may be controlled by the regulation of the four threaded screws, positioned at 90° from each other in the horizontal plane (see Fig. 3d). The contact surfaces between the sphere, the beam and the joint were spherically shaped in order to realize a self-centering system, at the same time obtaining a reduction of the contact pressure with respect to the case of a contact between non-spherical surfaces. The diameters of these spherical cavities are equal to 16 mm. During the tests, two steel spheres having a diameter of 15 mm were interposed to facilitate the self-centering of the specimen and to realize the external constraints at the same time. Two constraint conditions were realized during the experiments: pinned–pinned and pinned–clamped. In the former case, both the lower and the upper joints worked, through the steel spheres, as

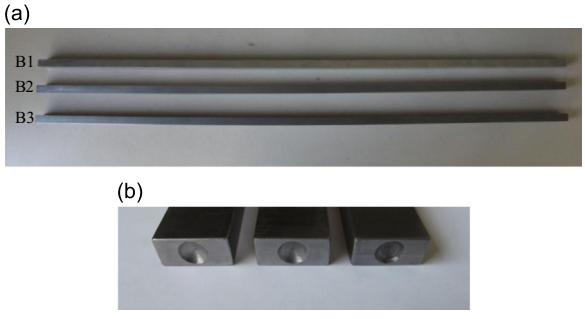


**Fig. 1.** Specimens with different geometrical deviations from the rectilinear condition, i.e., different ratios between the maximum offset at midlength, $e_0$, and the specimen length, $l$. (a) Rectified beam B1, with $e_0/l \leq 0.2/1000$, curved beam B2, with $e_0/l=1/1000$, and curved beam B3, with $e_0/l=2/1000$. (b) End cross-sections with spherical cavities of the three considered specimens.

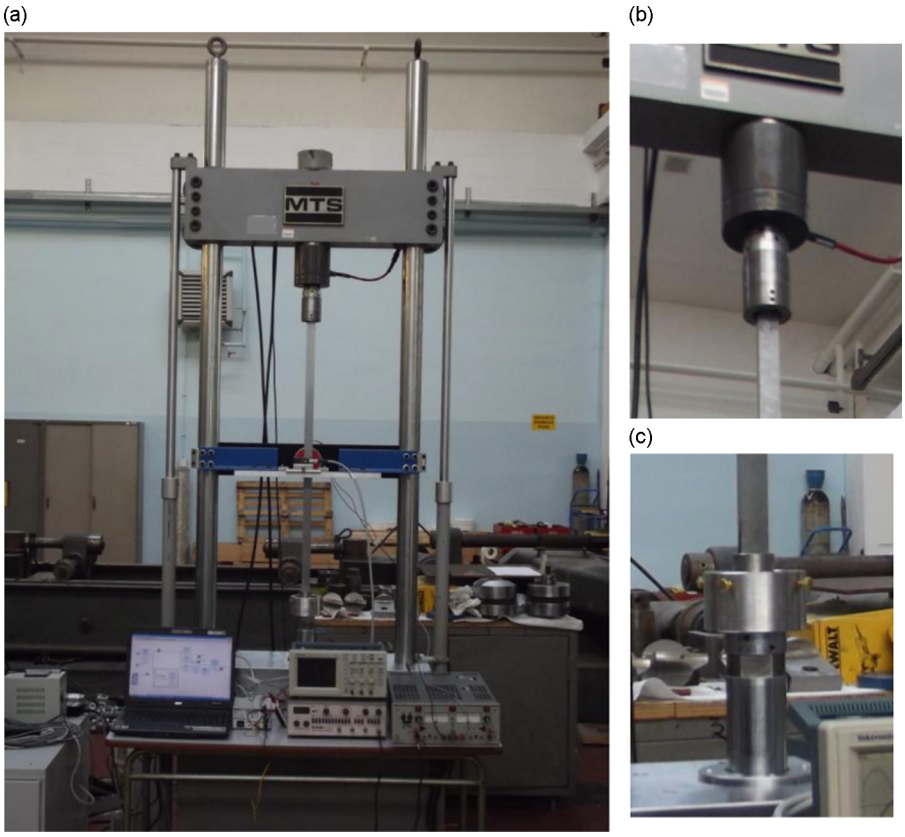


**Fig. 2.** General view of the experimental setup showing (a) the testing machine, a specimen, the experimental equipment, and the data acquisition system, (b) and (c) the upper and lower end joints, respectively, in the case of the hinged–hinged constraint condition.

spherical hinges that react only in compression (unilateral spherical hinges). In the pinned–clamped case, two steel plates were opportunely introduced and fixed into the upper joint in order to prevent, at least partially, end flexural rotations, while the lower joint remained unchanged.

The experimental equipment is shown in Fig. 5. It consists of two transverses connected each other by two aluminium circular joints that serve for connection to the testing machine frame. These joints have an external diameter of 120 mm and an internal one of 76.5 mm. On the transversal element presenting a C-shaped cross-section the electromagnet is fastened with a bolt in middle position, while the second transversal element is used to allocate the laser sensor. The latter is positioned on an adjustable sled, mounted on a sliding plate, in order to allow the regulation of the distance between the measuring point and the reflection surface. In particular, the inferior plate and the superior sled are used to regulate larger and smaller displacements, respectively. The characteristic response curves of electromagnet and laser sensor are reported in Fig. 6. The curve reported in Fig. 6a is related to experiments done on a ferromagnetic object at least 12 mm thick and with the electromagnet powered by direct current at a voltage of 24 V. The main default characteristics of the laser sensor are reported in Fig. 6b and in Table 1. During the experiments the default parameters were adopted.

The tests were performed controlling the vertical displacement transmitted by the linear actuator (hydraulic jack) to the beam (see Fig. 2c). The input was constituted by several steps of the imposed displacement and by the electromagnet forcing. The output was constituted by the time history of the beam midpoint transversal displacement, measured with the laser sensor disposed as shown in Fig. 7. Hence, for each imposed displacement the fundamental vibration frequency was obtained under both conditions of forced and free vibration. In the case of forced vibration, the electromagnet, disposed as shown in Fig. 7, transmitted to the beam a sinusoidal force, controlled in frequency and amplitude by the wave generator. In the case of free vibration, the electromagnet was turned off after 10 s and the free response was measured. Acquisition and analysis of the measured signals were carried out through computer programs that were specially developed using the software LabVIEW. A total of three independent methods were used to analyze the response, as it is described in Section 3.

## 3. Experimental results

A total of six testing configurations were performed changing the constraint conditions for each specimen (see Table 2). For each configuration, the fundamental vibration frequency was determined under different values of the mean axial force obtained imposing different vertical displacements to the beam end. The testing configurations are also schematically

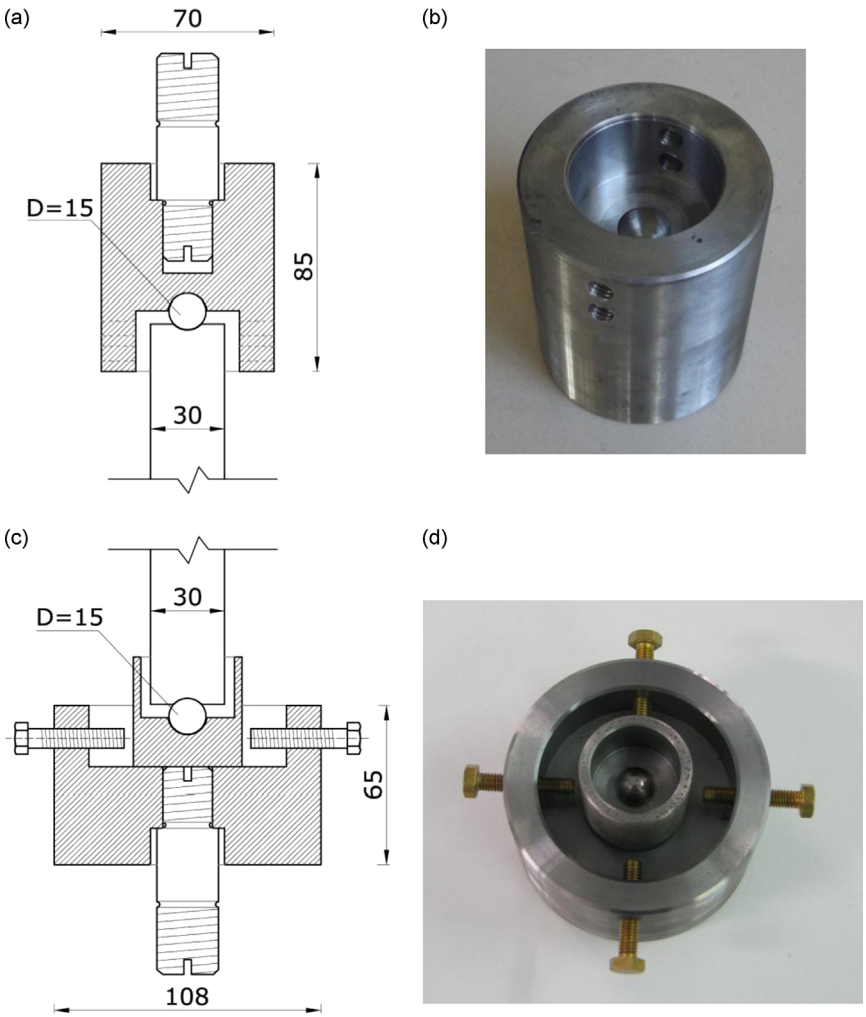


**Fig. 3.** Schemes and pictures of the end joints with indication of the main dimensions in mm. (a) and (b) upper constraint, that could be a unilateral spherical hinge or a partially fixed end. (c) and (d) lower constraint, adjustable in the horizontal plane, that always represents a unilateral spherical hinge

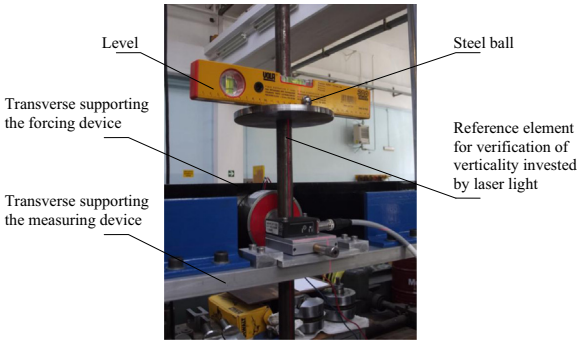


**Fig. 4.** Verification of the vertical alignment of the upper and lower end joints through a reference device coupled with a level and a self-levelling laser to guarantee the vertical positioning of the specimens and the correct transmission of the forces.

represented in Fig. 8 and reported in Table 2 according to their initial imperfection and considering the different constraints adopted.

Testing configurations 1 and 2 in Table 2, shown in Fig. 8a and b respectively, represent the cases in which the rectified beam is hinged at both the ends (case 1) and the case in which the upper end is clamped and the lower is hinged (case 2). The same constraint configurations are replicated for specimen B2, having a geometrical imperfection $e_0/l=1/1000$ (testing configurations 3 and 4 in Table 2), and for specimen B3, were $e_0/l=2/1000$ (testing configurations 5 and 6 in Table 2).

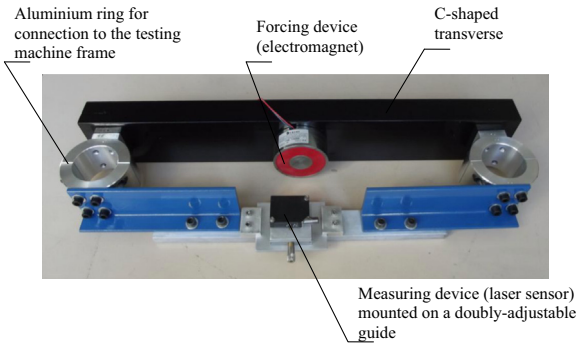


**Fig. 5.** Experimental equipment constituted by two aluminium rings for the connection to the testing machine frame, a C-shaped transverse by which the forcing device is supported, and an L-shaped transverse on which the measuring device is mounted.

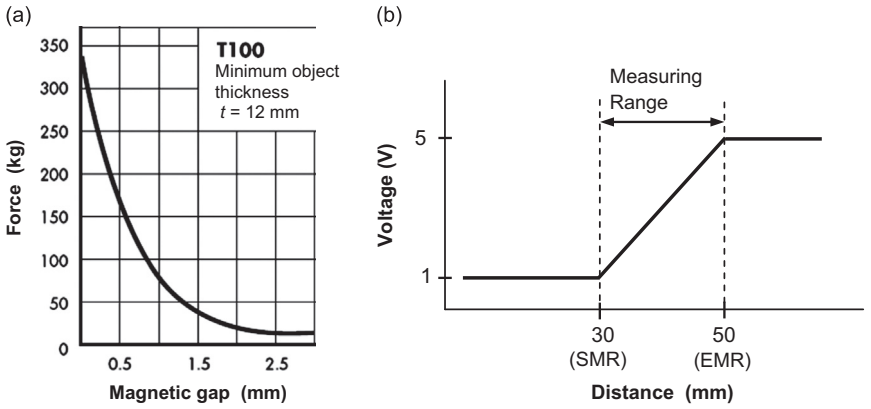


**Fig. 6.** Characteristic curves of (a) electromagnet and (b) laser sensor with indication of Start of Measuring Range (SMR) and End of Measuring Range (EMR).

**Table 1**
Main characteristics of the laser sensor.

| Measuring range (MR) | Start of measuring range (SMR) | Midrange (MR) | End of measuring range (EMR) | Resolution (Dynamic 750 Hz) |
|---|---|---|---|---|
| 20 mm | 30 mm | 40 mm | 50 mm | 10 μm |

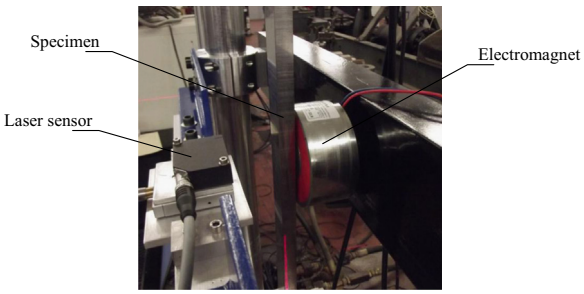


**Fig. 7.** Testing configuration with rectified beam (specimen B1) undergoing post-critical deflections.

In the case of double-hinged beam the theoretical buckling load calculated according to Euler's formula [37] is about 17.5 kN, while the theoretical fundamental flexural frequency according to linear dynamics [1,2] is about 35.2 Hz. On the other hand, in the case of hinged–clamped beam, Euler's critical load is about 37.2 kN, while the fundamental frequency is 55 Hz. The previous theoretical values are not affected by imperfections and so they hold for all specimens B1, B2, and B3. First, the axial load versus transversal displacement curves were obtained for all the tested configurations as a preliminary phase (Fig. 9). The axial load is intended to be the specimen reaction which corresponds to the axial displacement imposed

**Table 2**
Testing configurations.

| Testing configuration | Specimen | Geometrical deviation ($e_0/l$) | Upper-constraint condition* |
|---|---|---|---|
| 1 | B1 | $\leq 0.2/1000$ | Hinged |
| 2 | B1 | $\leq 0.2/1000$ | Partially clamped |
| 3 | B2 | 1/1000 | Hinged |
| 4 | B2 | 1/1000 | Partially clamped |
| 5 | B3 | 2/1000 | Hinged |
| 6 | B3 | 2/1000 | Partially clamped |

* The lower joint is always a unilateral spherical hinge in all the testing configurations.

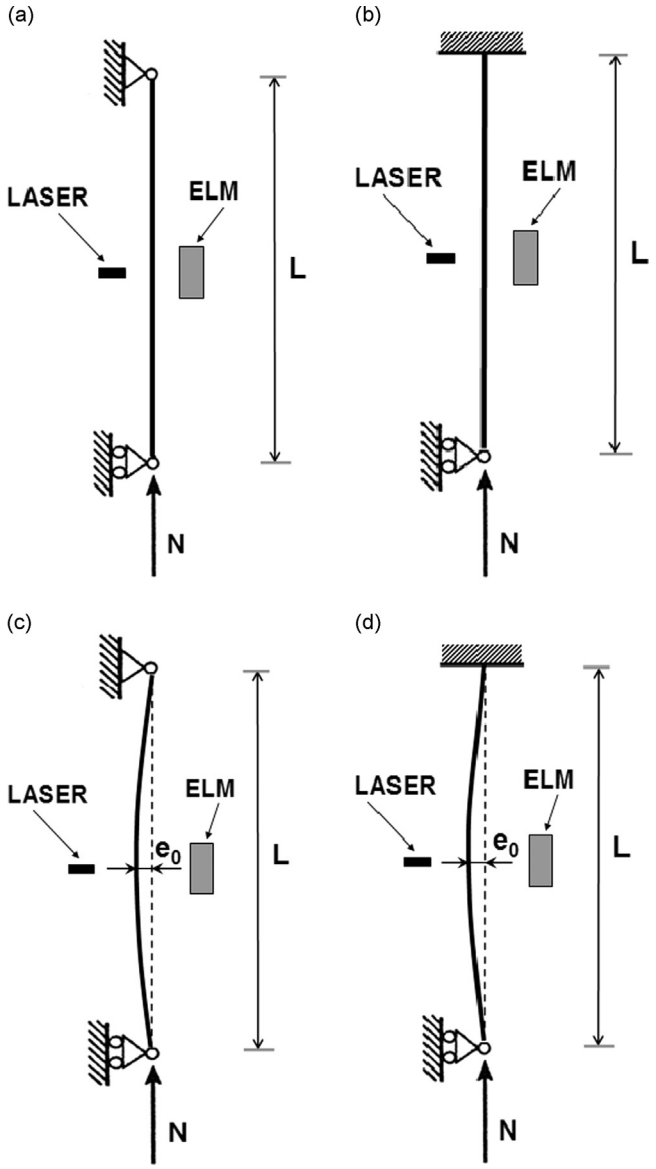


**Fig. 8.** Schematic representation of the testing configurations. (a) Double-hinged rectified beam (configuration 1 in Table 2), (b) hinged–clamped rectified beam (configuration 2 in Table 2), (c) double-hinged imperfect beam (configurations 3 and 5 in Table 2), and (d) hinged–clamped imperfect beam (configurations 4 and 6 in Table 2).

by the actuator of the testing machine: therefore, its value came from the MTS. The transversal displacement is intended to be the midpoint deflection of the specimen: its value was measured with the laser sensor. The curves reported in Fig. 9 are obtained by applying a ramp to the displacement of the lower actuator with an imposed velocity of $25 \times 10^{-6}$ m/s.

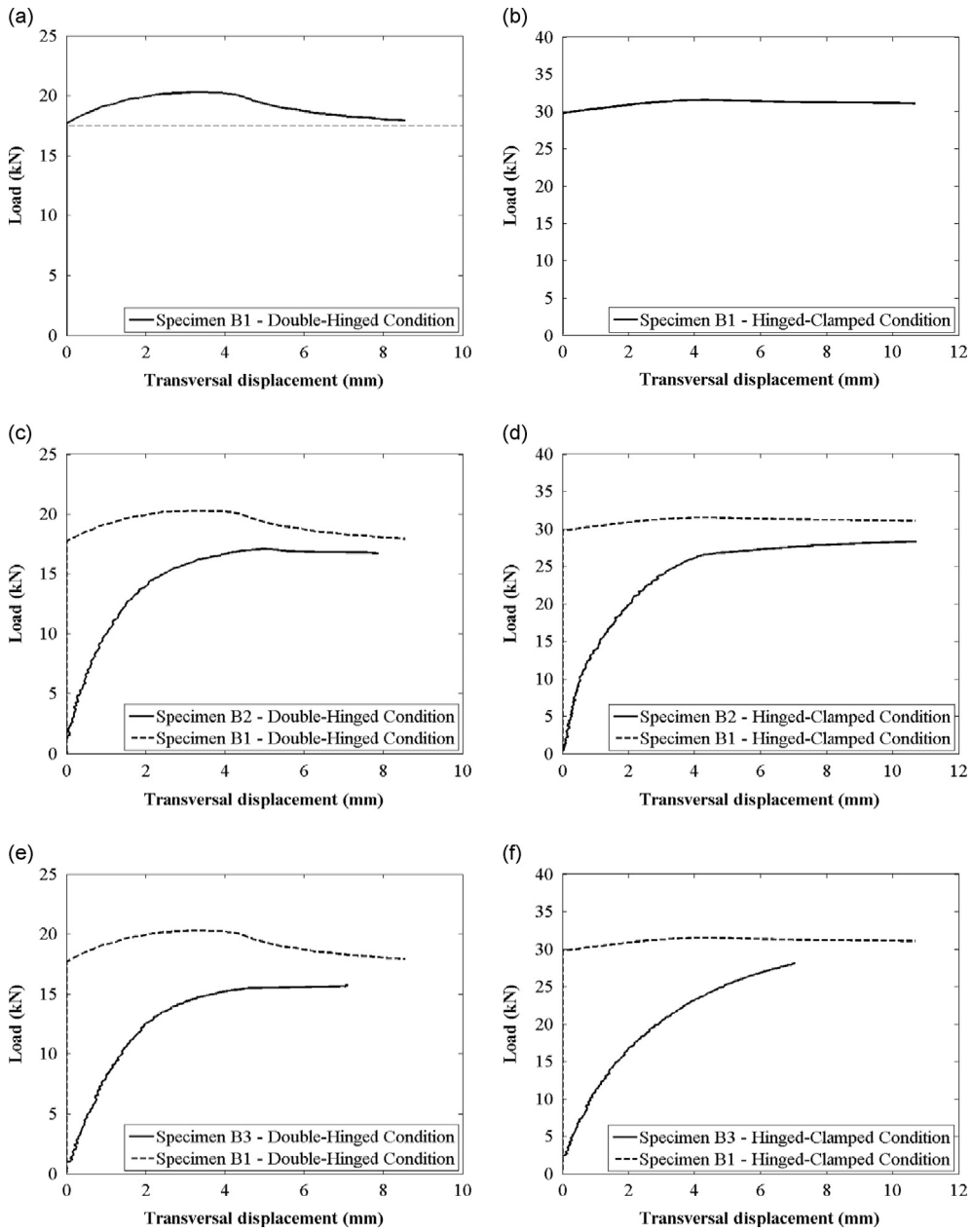


**Fig. 9.** Load versus transversal displacement curves for specimens B1–3 under different constraint conditions. (a) Specimen B1 (rectified beam) in the double-hinged constraint condition, (b) specimen B1 in the hinged–clamped constraint condition, (c) specimen B2 (1/1000) compared with specimen B1 in the double-hinged constraint condition, (d) specimen B2 compared with specimen B1 in the hinged–clamped constraint condition, (e) specimen B3 (2/1000) compared with specimen B1 in the double-hinged constraint condition, and (f) specimen B3 compared with specimen B1 in the hinged–clamped constraint condition.

Fig. 9a shows the load versus transversal displacement for the double-hinged rectified beam (case 1 in Table 2). This graph represents the typical response of a perfect beam, showing a bifurcation point almost equal to the theoretical Euler's buckling load (17.5 kN). The post-critical response is also reported, showing a stable post-critical branch, exhibiting an hardening phase and then a softening behavior which asymptotically reaches the critical load.

Fig. 9b shows the load versus transversal displacement of the same beam but considered in the case of hinged–clamped constraint condition (case 2 in Table 2). In this case larger differences between the expected and the measured results were obtained. In fact, the graph shows a bifurcation in correspondence of a load equal to about 30 kN, while the theoretical Euler's load is equal to 37.2 kN. This behavior can be interpreted as an inefficiency of the constraint condition at the upper end with a condition of not-perfectly-clamped joint. Fig. 9c, d show in solid line the load vs. displacement curves for the first curved beam (cases 3 and 4 in Table 2, respectively). In both the double-hinged (Fig. 9c) and hinged–clamped (Fig. 9d) cases

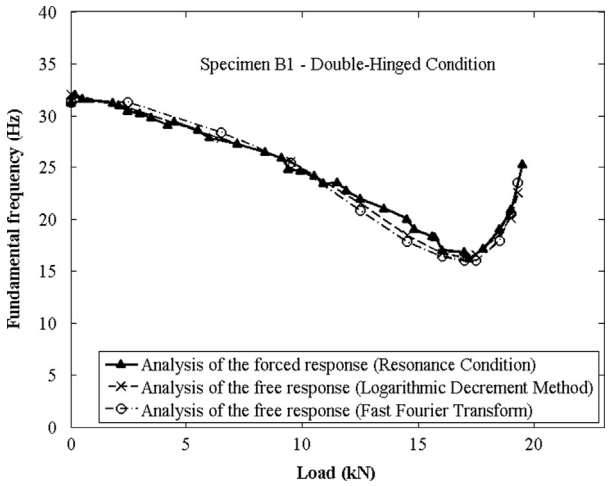


**Fig. 10.** Fundamental frequency versus axial load curves for the testing configuration 1 in Table 2 (specimen B1, double-hinged condition) obtained applying three different procedures: the analysis of the forced response corresponding to different frequencies of the harmonic excitation, through which the resonance condition may be detected; the analysis of the free response applying the Logarithmic Decrement Method; and the analysis of the free response using the Fast Fourier Transform.

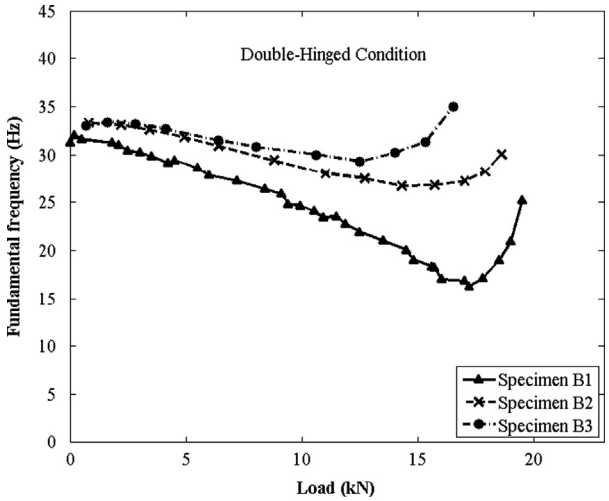


**Fig. 11.** Fundamental frequency versus axial load curves for specimens B1–3 in the double-hinged constraint condition (only the values obtained by the analysis of the forced response are reported).

the response is the typical one of beams with initial imperfections. Transversal displacements appear from the beginning and increase more than proportionally with the load due to second-order effects that reduce the flexural stiffness. When the flexural stiffness approaches zero, the maximum loading capacity is reached. The load vs. displacement curves for specimen B3, under testing conditions 5 and 6 in Table 2, are reported in Fig. 9e, f, respectively. In these cases, responses analogous to those observed for specimen B2, reported in Fig. 9c, d, were observed. For specimen B3 the effects of the initial imperfection are larger respect to specimen B2, although the behavior is similar. In all the cases presenting initial deformation, the maximum load never reaches the equivalent value of the rectified beam (testing configurations 1 and 2 in Table 2). In order to appreciate these differences, in Fig. 9c–f the corresponding curves of the rectified beam are also reported (dashed lines).

Fig. 10 shows the curves fundamental frequency versus axial load for the case 1 listed in Table 2. The natural fundamental frequencies were obtained by applying three different and independent procedures. Lines marked with solid triangles are related to the fundamental frequencies obtained identifying the resonance condition, i.e. analyzing the forced response corresponding to different frequencies of the harmonic excitation transmitted by the electromagnet. Lines marked with crosses correspond to the fundamental frequencies obtained applying the Logarithmic Decrement Method [1] to the free response signal. Lastly, lines marked with white circles are referred to the fundamental frequencies obtained performing the Fast Fourier Transform of the free response signal. In all the analyzed cases (1–6 in Table 2), there is a perfect correspondence between the results given by the three adopted methods.

First of all, we observe that the zero-frequency condition is never reached, due to the combined effects of the geometric and material imperfections (the rectified beam is not a perfect beam in reality) and of the corresponding non-trivial equilibrium path associated to the imposed displacement. Nevertheless, a distinction between the pre- and the post-critical phases is however possible. In fact, two different trends of the natural frequency with respect to the axial load were observed, and the minimum in the curve identifies the critical state. It is possible to observe that the transition from the first phase to the second is particularly sharp for the rectified beam, while it becomes smoother in the cases of beams presenting larger initial curvature. Moreover, an important influence of the initial imperfections on the evolution of the natural frequency can be observed.

Fig. 11 shows the variation of the fundamental frequency versus the axial load for specimens B1–3 in the double-hinged constraint condition (cases 1, 2, and 3 in Table 2), while the same curves for specimens B1–3 in the hinged–clamped constraint condition are reported in Fig. 12 (cases 2, 4, and 6 in Table 2). For all these tests the qualitative trend of the fundamental frequency shows a decrease down to the minimum of the curve, after which the natural frequency starts to increase sharply, showing a stiffening behavior. In this case of displacement controlled experiments the response is always

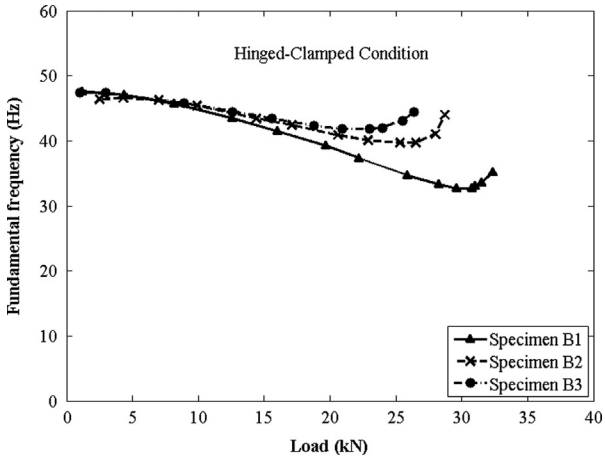


**Fig. 12.** Fundamental frequency versus axial load curves for specimens B1–3 in the hinged–clamped constraint condition (only the values obtained by the analysis of the forced response are reported).

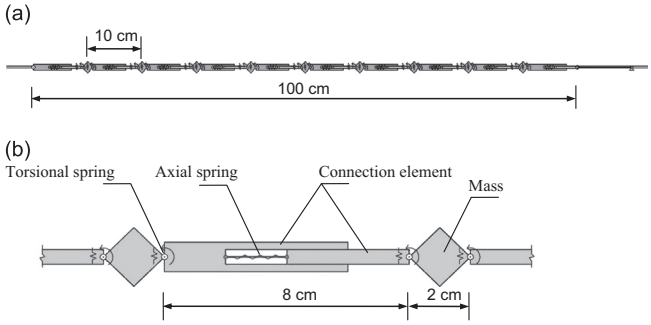


**Fig. 13.** Multi-body model of a specimen obtained with Working Model 2D 5.0. (a) General view of the complete model showing nine masses (squares) and the connecting elements. (b) Detail of a portion showing masses, a massless connection element, axial and torsional springs that simulate the axial and flexural elastic stiffness of the entire beam.

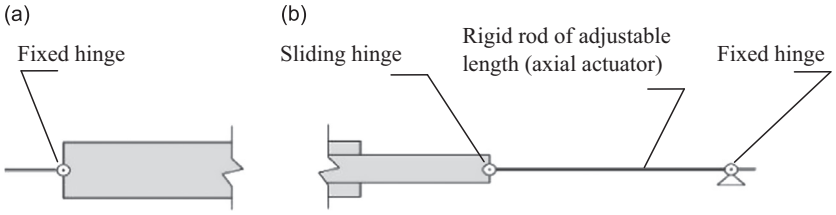


**Fig. 14.** External constraints simulating the end connections (upper and lower joints) of the experimental tests. (a) Fixed hinge simulating the upper joint. (b) Sliding hinge simulating the lower joint connected to a rod element that simulates the linear actuator of the testing machine (hydraulic jack).

stable, but after a certain value of the transversal displacement the tendency is reversed. In the first phase, the specimens follow a straight beam-like behavior, showing a reduction in the fundamental frequency as the axial compression load increases. During the second phase, the specimens exhibit an arch-like (curved beam-like) behavior, showing a stiffening leading to an increase in the fundamental frequency.

The behavior observed for specimen B1 in the double-hinged condition (case 1 in Table 2) is characterized by two well distinguishable phases. In this case, the transition between a pseudo-linear branch and a pseudo-exponential one is particularly marked (see Figs. 10 and 11). From this point of view the transition is sharp and the point in the curve

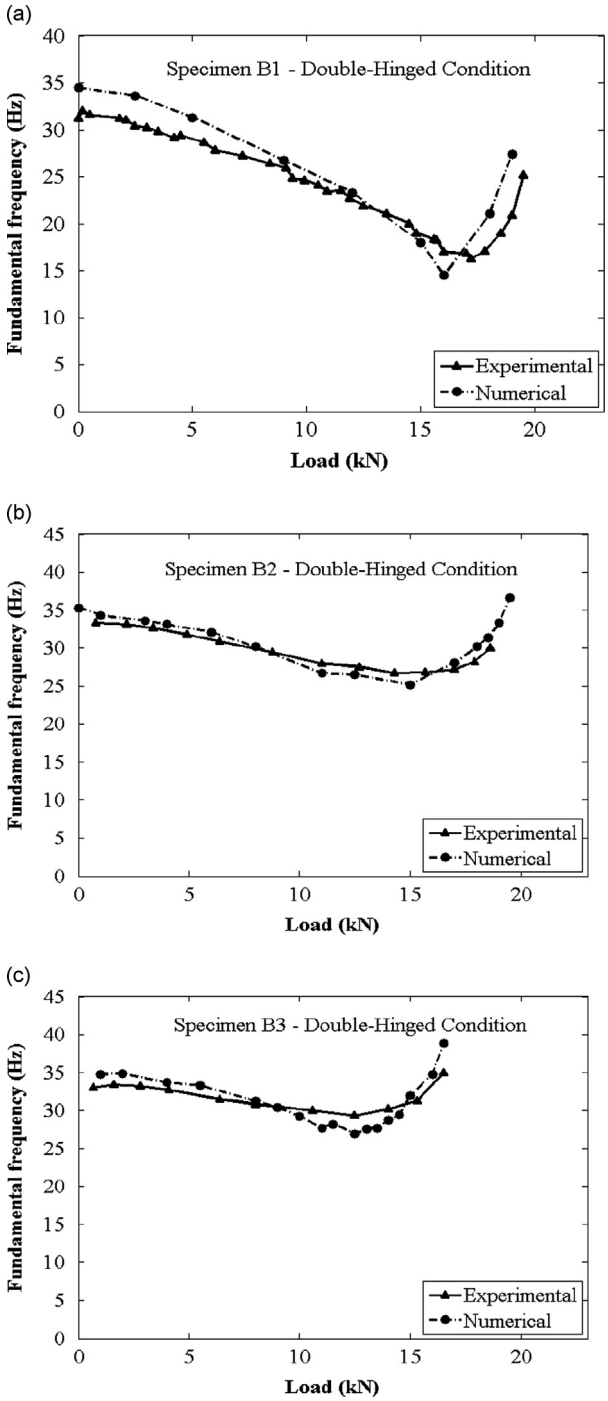


**Fig. 15.** Comparison between experimental and numerical fundamental frequency versus axial load curves for specimens (a) B1, (b) B2, and (c) B3 in the double-hinged constraint condition.

corresponding to 17.2 kN and 16.2 Hz is unpredictable. Under the same constraint condition, specimens B2 and B3 (cases 3, and 5 in Table 2) show a wider transition interval with respect to specimen B1. The greater the initial geometrical deviation the smaller the slope in the first branch of the frequency trend and the smoother the transition phase (see Fig. 11). The possibility of anticipating the transition point when the acting load is far from the critical value could be used in analogous measurements performed on slender elements subjected to subsidence imposed in situ in order to monitor their stability. Analogous considerations could be done in the case of hinged–clamped configurations (see Fig. 12).

## 4. Numerical simulations

Numerical models were implemented in order to reproduce the experimental tests conducted on specimens B1, B2 and B3 in the double-hinged condition (testing configurations 1, 3, and 5 in Table 2). The simulations were performed using Working Model 2D, a multi-body dynamic simulator based on the numerical solution of the equations of motion. Fig. 13a shows a general view of the model reproducing the rectified beam (specimen B1), hinged at both the ends, in the undeformed configuration. The model is constituted by nine elements where the mass is concentrated, ten massless connection units, ten axial springs, eighteen torsional springs, two end constraints, and, lastly, a rod element through which we were able to simulate the effect of the hydraulic jack. The model concentrates the mass of the specimen into nine squared masses, each one being two centimeters long and having a mass equal to one ninth of the specimen's total mass; in particular, the value was set up equal to $3.09 \times 10^{-3}$ kg. The masses are connected to each other through connection units that are massless and infinitely rigid in flexure, but at the same time they allow axial displacements (see Fig. 13b). The axial stiffness of the specimen is concentrated in ten axial springs, placed inside the connection units. These springs present a relaxed length of two centimeters and a linear stiffness equal to $9.45 \times 10^{8}$ N/m. The flexural stiffness of the specimen is concentrated into the torsional springs connecting the masses to the rigid massless elements (see Fig. 13b). Each torsional spring has a linear stiffness equal to $6.0 \times 10^{4}$ Nm/rad. The values assigned to the stiffness of the axial and torsional springs were evaluated in order to model correctly the axial and bending stiffness of the specimen, therefore reproducing the values of fundamental frequency and buckling load.

The external constraints are represented by two hinges, one of which is fixed and simulates the upper joint, while the other one can slide on a guide in order to simulate the lower joint. (see Figs. 2 and 14). The hydraulic jack is simulated by means of an infinitely rigid rod element, whose length could be adjusted in order to reproduce the imposed displacements obtained experimentally. In this way, the software has enabled us to simulate the way the displacement was imposed by the testing machine during the experiments.

The numerical models allowed the simulation of the response of the three specimens B1, B2, and B3, with their geometrical imperfections. Specimen B1 (rectified beam) was considered perfectly straight, and its initial configuration was assumed rectilinear. For specimens B2 and B3 an originally curved shape was generated to reproduce the imperfect geometry of the two specimens. This approximation was very close to the experimental conditions realized in the laboratory and it allowed us to obtain a good numerical reproduction of the experimental results. Therefore, for each imposed displacement, the fundamental vibration frequency was obtained by analyzing the time history of the transversal displacement of the central mass. The initial condition was represented by a deformed shape similar to the first vibration mode of the beam, with zero-velocity. The maximum amplitude imposed in the initial condition was equal to 2 mm (displacement of the central mass), in all the simulations.

As regards to the numerical procedure and the simulation accuracy adopted for the solution, among the possibilities offered by the software, we chose the following custom settings. Regarding the Animation Step, we set the value $5 \times 10^{-6}$ s. This value defines the time between frames of animation. For the Integrator Error, we set the value $2 \times 10^{-5}$ m. This value,

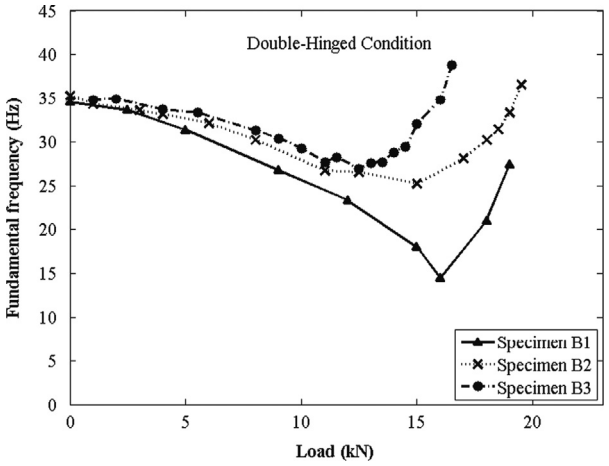


**Fig. 16.** Comparison between numerical fundamental frequency versus axial load curves for specimens B1–3 in the double-hinged constraint condition.

referred to the configuration (position), provides an absolute error bound for variable step integration. Concerning the Integrator settings, we selected the Kutta–Merson integrator, which adopts an integration scheme which yields highly accurate results fairly quickly. About the Integration Step settings, we chose the variable mode. In this way, the integrator automatically adjusts the time step throughout the simulation to optimize computational performance. The integration step may become smaller than the one specified in the Animation Step, but will never become larger. Lastly, as regards to other settings, we selected the Automatic mode for both Overlap Error and Assembly Error, while we set the value 10 in the Significant digits box.

Fig. 15 shows the comparison between the experimental results and those obtained by the numerical simulations. It is possible to observe that fundamental frequency versus load behaviors obtained during the tests are well reproduced by the numerical model. In the case of specimen B1 (rectified beam), in particular, the frequency trend obtained increasing the imposed displacement is well reproduced showing an abrupt transition from the first to the second phase. The cusp localized approximately in correspondence of 16 kN is even more evident than in the experimental plot (see Fig. 15a), consistently with the approximation of the numerical model. Similar results were obtained in the cases of the simulations reproducing the tests on specimens B2 and B3 (see Fig. 15b, c).

Fig. 16 collects all the fundamental frequency versus load curves obtained by the numerical simulations. From these graphs it is possible to observe that all the aspects originally observed from the experimental results are therefore confirmed and reproduced by the numerical simulations.

In conclusion, the implemented numerical models were able to describe the most important features characterizing the frequency vs. load evolution in slender elements subjected to imposed displacements, showing a good agreement with the experiments. An improvement of the closeness of the numerical values to the experimental ones could be obtained by refining the models. A larger number of elements, as well as a better fitting of the numerical values attributed to mass and stiffness of each component should induce a better reproduction of the experiments. Finally, models like those implemented in the present study may be useful to predict, by simulating laboratory tests, the behavior of structural elements to obtain indications in designing new structures and components or to offer a valid interpretation to experimental measurements carried out on existing structures subjected to imposed displacements or constraint settlements.

## 5. Conclusions

In this study, the evolution of the fundamental frequency in slender beams subjected to axial end displacements is experimentally investigated. Three elements with different initial curvatures were tested in the pinned–pinned and pinned–clamped constraint conditions, and therefore results were compared. It can be noted that a first phase, where the fundamental frequency decreases with the axial load, is followed by a stiffening one, where the trend is reversed. The geometric imperfection (initial curvature) reduces the negative slope of the softening branch, therefore anticipating the transition point and making this transition smother at the same time. These type of behavior, analytically predicted by previous studies [45,47] for other profiles of the initial imperfection and end conditions, must be well taken into account when designing new structures as well as in monitoring existing ones. The possibility to reproduce the experimental results through numerical simulations allows a valid interpretation for in-situ measurements, or even to perform virtual laboratory tests. This approach could be used to interpret the behavior of more complicated structural systems subjected to imposed displacements or affected by subsidence of the external constraints.

## Acknowledgments

Special thanks are due to Ind. Eng. F. Alasia for his valuable cooperation during the phases of design and set-up of the experimental tests.

## References

[1] R.W. Clough, J. Penzien, *Dynamics of Structures*, McGraw-Hill, New York, 1975.
[2] W. Weaver Jr., S.P. Timoshenko, D.H. Joung, *Vibration Problems in Engineering*, 5th ed. John Wiley & Sons, 1990 (Wiley).
[3] I.A. Karnovsky, O.I. Lebed, *Formulas for Structural Dynamics: Tables, Graphs and Solutions*, McGraw-Hill, New York, 2000.
[4] L.N. Virgin, *Vibration of Axially Loaded Structures*, Cambridge University Press, New York, 2007.
[5] C. Massonnet, The relations between the normal modes of vibration and stability of elastic systems. Bulletin des Cours et des Laboratoires D'Essais des Constructions du Génie Civil et d'Hydraulique Fluviale (Bulletin du C.E.R.E.S.) 1, 1940.
[6] O. Belluzzi, On the vibration period of a structure in presence of compressive axial loads (in Italian), *Giornale del Genio Civile* 4 (1951).
[7] H. Lurie, Lateral vibrations as related to structural stability, *Journal of Applied Mechanics* 19 (1952) 195–204.
[8] A.E. Galef, Bending frequencies of compressed beams, *Journal of Acoustical Society of America* 44 (8) (1968) 643.
[9] A. Bokaian, Natural frequencies of beams under compressive axial loads, *Journal of Sound and Vibration* 126 (1) (1988) 49–65.
[10] A. Bokaian, Natural frequencies of beams under tensile axial loads, *Journal of Sound and Vibration* 142 (3) (1990) 481–498.
[11] H. Abramovich, Natural frequencies of Timoshenko beams under compressive axial loads, *Journal of Sound and Vibration* 57 (1) (1992) 183–189.
[12] H. Matsunaga, Free vibration and stability of thin elastic beams subjected to axial forces, *Journal of Sound and Vibration* 191 (5) (1996) 917–933.
[13] L.W. Chen, G.S. Shen, Vibration and buckling of initially stressed curved beams, *Journal of Sound and Vibration* 215 (3) (1998) 511–526.
[14] E. Carrera, A study of transverse normal stress effect on vibration of multilayered plates and shells, *Journal of Sound and Vibration* 225 (5) (1999) 803–829.

[15] H. Matsunaga, Vibration and buckling of deep beam-columns on two-parameter elastic foundations, *Journal of Sound and Vibration* 228 (2) (1999) 359–376.
[16] R.C. Batra, S. Vidoli, F. Vestroni, Plane wave solutions and modal analysis in higher order shear and normal deformable plate theories, *Journal of Sound and Vibration* 257 (1) (2002) 63–88.
[17] V.H. Cortinez, M.T. Piovan, Vibration and buckling of composite thin-walled beams with shear deformability, *Journal of Sound and Vibration* 258 (4) (2002) 701–723.
[18] W. Lacarbonara, A. Paolone, H. Yabuno, Modeling of planar nonshallow prestressed beams towards asymptotic solutions, *Mechanics Research Communications* 31 (2004) 301–310.
[19] J.D. Aristizabal-Ochoa, Timoshenko beam-column with generalized end conditions and nonclassical modes of vibration of shear beams, *ASCE Journal of Engineering Mechanics* 130 (10) (2004) 1151–1159.
[20] D. Addessi, W. Lacarbonara, A. Paolone, On the linear normal modes of planar pre-stressed curved beams, *Journal of Sound and Vibration* 284 (2005) 1075–1097.
[21] D. Addessi, W. Lacarbonara, A. Paolone, Free in-plane vibrations of highly buckled beams carrying a lumped mass, *Acta Mechanica* 180 (2005) 133–156.
[22] S.M. Kim, Stability and dynamic response of Rayleigh beam–columns on an elastic foundation under moving loads of constant amplitude and harmonic variation, *Engineering Structures* 27 (2005) 869–880.
[23] L.G. Arboleda-Monsalvea, D.G. Zapata-Medina, J.D. Aristizabal-Ochoa, Stability and natural frequencies of a weakened Timoshenko beam-column with generalized end conditions under constant axial load, *Journal of Sound and Vibration* 307 (2007) 89–112.
[24] L.G. Arboleda-Monsalve, D.G. Zapata-Medina, J.D. Aristizabal-Ochoa, Timoshenko beam-column with generalized end conditions on elastic foundation: dynamic-stiffness matrix and load vector, *Journal of Sound and Vibration* 310 (2008) 1057–1079.
[25] J. Yang, Y. Chen, Y. Xiang, X.L. Jia, Free and forced vibration of cracked inhomogeneous beams under an axial force and a moving load, *Journal of Sound and Vibration* 312 (2008) 166–181.
[26] Y.Q. Zhang, Y. Lu, S.L. Wang, X. Liu, Vibration and buckling of a double-beam system under compressive axial loading, *Journal of Sound and Vibration* 318 (2008) 341–352.
[27] Y. Fridman, H. Abramovich, Enhanced structural behaviour of flexible laminated composite beams, *Composite Structures* 82 (2008) 140–154.
[28] J.F. Monsalve-Cano, J.D. Aristizabal-Ochoa, Stability and free vibration analyses of an orthotropic singly symmetric beam-column with generalized end conditions, *Journal of Sound and Vibration* 328 (2009) 467–487.
[29] T.P. Vo, J. Lee, K. Lee, On triply coupled vibrations of axially loaded thin-walled composite beams, *Computers and Structures* 88 (2010) 144–153.
[30] C. Li, C.W. Lim, J.L. Yu, Q.C. Zeng, Analytical solutions for vibration of simply supported nonlocal nanobeams with an axial force, *International Journal of Structural Stability and Dynamics* 11 (2) (2011) 257–271.
[31] E. Lofrano, A. Paolone, G. Ruta, A numerical approach for the stability analysis of open thin-walled beams, *Mechanics Research Communications* 48 (2013) 76–85.
[32] L. Jun, H. Hongxing, Free vibration analysis of axially loaded laminated composite beams based on higher-order shear deformation theory, *Meccanica* 46 (6) (2011) 1299–1317.
[33] A. Carpinteri, M. Paggi, A theoretical approach to the interaction between buckling and resonance instabilities, *Journal of Engineering Mathematics* 78 (1) (2013) 19–35. (ISSN 0022-0833).
[34] V.V. Bolotin, *Nonconservative Problems of the Theory of Elastic Stability*, Pergamon Press, New York, 1963.
[35] V.V. Bolotin, *The Dynamic Stability of Elastic Systems*, Holden-Day, San Francisco, 1964.
[36] K. Useyin, Dynamics, stability, and bifurcations, *ASME Applied Mechanics Reviews* 55 (2002) R5–R15.
[37] Z.P. Bažant, L Cedolin, *Stability of Structures*, Dover, Mineola, 2003.
[38] W.C. Xie, *Dynamic Stability of Structures*, Cambridge University Press, New York, 2011.
[39] O. Belluzzi, On the experimental determination of the critical load through vibration tests (in Italian), *Ingegneri-Architetti-Costruttori* 4 (1951).
[40] I.I. Anik'ev, M.I. Mikhailova, E.A. Sushchenco, Nondestructive determination of the critical load of column-type structures, *International Applied Mechanics* 30 (12) (1994) 990–994.
[41] I.I. Anik'ev, E.A. Sushchenko, Experimental nondestructive determination of critical loads on thin-walled structures, *International Applied Mechanics* 38 (4) (2002) 485–488.
[42] S. Woinowsky-Krieger, The effect of an axial force on the vibration of hinged bars, *Journal of Applied Mechanics* 17 (1950) 35–36.
[43] D. Burgreen, Free vibrations of a pin-ended column with constant distance between pin ends, *Journal of Applied Mechanics* 18 (1951) 135–139.
[44] S.M. Dickinson, The lateral vibration of slightly bent slender beams subject to prescribed axial end displacement, *Journal of Sound and Vibration* 68 (4) (1980) 507–514.
[45] C.S. Kim, S.M. Dickinson, The flexural vibration of slightly curved slender beams subject to axial end displacement, *Journal of Sound and Vibration* 104 (1) (1986) 170–175.
[46] N. Yamaki, A. Mori, Non-linear vibrations of a clamped beam with initial deflection and initial axial displacement, part I: theory, *Journal of Sound and Vibration* 71 (3) (1980) 333–346.
[47] S. Ilanko, The vibration behaviour of initially imperfect simply supported beams subject to axial loading, *Journal of Sound and Vibration* 142 (2) (1990) 355–359.
[48] W.L. Hallauer, C. Ma, On the mechanical behavior of slender, slightly curved, compressed microbridges, *Journal of Micromechanics and Microengineering* 21 (6) (2011). 065025(12pp.). http://dx.doi.org/10.1088/0960-1317/21/6/065025.